

# Asymmetric dynamical localization and precision measurement of BEC micromotion

S. Sagar Maurya, J. Bharathi Kannan, Kushal Patel, Pranab

Dutta, Korak Biswas, M. S. Santhanam,<sup>\*</sup> and Umakant D. Rapol<sup>†</sup>

*Department of Physics, Indian Institute of Science Education and Research, Pune 411008, India*

(Dated: June 21, 2024)

We show that a Bose-Einstein Condensate (BEC) launched with non-zero initial momentum into a periodically kicked optical lattice creates an asymmetrically localized momentum distribution in a moving frame with a small initial current. This asymmetric localization is investigated under two scenarios; (a) when the BEC is in motion in the laboratory frame and, (b) when the optical lattice is in motion in the laboratory frame. The asymmetric features are shown to arise from the early-time dynamics induced by the broken parity symmetry and, asymptotically, freeze as the dynamical localization stabilizes. The micromotion of BEC is measured using the early-time asymmetry. In this context, micromotion refers to the extremely low initial velocity of the BEC along the lattice direction. This originates from the jitter when the hybrid trap potential is turned off. By employing BEC in a kicked and moving optical lattice, the asymmetry in early-time dynamics is measured to precisely characterize and quantify the micromotion phenomena in the quantum system. Micromotion measurement has applications in quantifying systematic shifts and uncertainties in light-pulse interferometers.

PACS numbers: physics

## I. INTRODUCTION

In recent years, there has been much interest in studying quantum kicked rotor (QKR) with BEC – with and without tunable interactions [1–4]. Further, the ease of imprinting the lattice phase on the BEC also provides different types of effects such as on-resonance quantum ratchets [5, 6] and quantum boomerang effect [7–9]. BEC based QKR has also been utilized in coupled quantum kicked rotors [1] where two incommensurate optical lattices drive a quantum to classical transition by breaking dynamical localization (DL). A discrete-time quantum walk has also been observed in the BEC-based system [10]. Here, we employ a QKR test-bed based on a BEC to experimentally demonstrate the asymmetric dynamical localization and we utilize this feature to perform precision measurement of BEC micromotion.

Precision measurements with light-pulse atom interferometers have opened tremendous applications in quantum sensing [11–13]. Atom interferometers are successfully utilized in gravimetry [13–15], rotation sensing [16, 17], magnetometers [18], and the determination of photon recoil [19]. Particularly in precision rotation sensing and gravimetry, nullifying the systematic shifts and measurement errors coming from Coriolis effect [20] in phase shifts necessitates precise knowledge of the initial velocity [14, 16, 21]. This initial velocity may arise from external launch velocities or micromotion coming from small movement of the atomic cloud during the turnoff of the trapping potential. In a rotation sensor, the phase shift caused due to this initial velocity adds to the Sagnac phase shift [20]. The Sagnac phase shift is in the range of

tens of milliradians (mrad) for a velocity of 100  $\mu\text{m/s}$  over an interferogram time of hundreds of milliseconds (ms). The velocity range of micromotion can lie in the range of 100-1000  $\mu\text{m/s}$ , which is much smaller compared to the velocity imparted due to two-photon recoil momentum ( $\approx 1 \text{ cm/s}$ ). The measurement of such a small velocity is challenging and requires huge time-of-flight in standard absorption imaging or very precise Bragg or Raman spectroscopy to measure the Doppler shift [21–23].

Firstly, we experimentally demonstrate localization in momentum space by launching the BEC with varying initial momentum or by inducing the lattice motion. A constant phase evolution of the launched wave function or the lattice motion creates an asymmetric momentum distribution. Furthermore, we illustrate that the asymmetric nature of the momentum distribution can be easily controlled by adjusting the launch momentum rather than altering the direction of the launch momentum. In contrast to previous studies [24] with cold atoms, where such asymmetry arises from pulse shape effects and observed after long time, here we demonstrate that such asymmetry arises much earlier in time [5, 7] and the asymmetry gets settled as dynamical localization takes place. An asymmetry in the localized state has been reported in Ref.[7] in a BEC by single phase change and phase reversal in the beginning. By utilizing this asymmetric behaviour of the localization in the early-time dynamics, we present a method to measure the micromotion of the BEC [25–27] in an Atom Optics Kicked Rotor (AOKR). The AOKR is already utilized for measurement of gravity through survival resonances [28, 29]. We demonstrate that even this micromotion of the BEC can induce early-time asymmetry in the momentum distribution. This asymmetry directly quantifies the velocity of micromotion, aligning with the primary focus of the current study.

<sup>\*</sup> [santh@iiserpune.ac.in](mailto:santh@iiserpune.ac.in)

<sup>†</sup> [umakant.rapol@iiserpune.ac.in](mailto:umakant.rapol@iiserpune.ac.in)

## II. QKR IN MOVING OPTICAL LATTICE

The quantum kicked rotor (QKR) is a fundamental model of quantum chaos [30] extensively explored for its demonstration of dynamical localization [31, 32]. The classical kicked rotor can display chaotic dynamics accompanied by a diffusive growth of mean energy. Over extended time scales, quantum interference effects inhibit classical diffusive dynamics, a phenomenon in momentum space analogous to Anderson localization [33]. Since the first realization of the QKR using cold atoms [34], QKR has spurred numerous experimental investigations to explore a variety of scenarios that inhibit localization [35–37]. Physically, the standard kicked rotor describes a particle subjected to periodic kicks imparted by the stationary optical lattice created by counter-propagating laser beams. However, in this work, we consider a kicked rotor system in which the optical lattice moves at a constant velocity in the laboratory frame. The Hamiltonian of QKR in a moving lattice is given by [38]

$$H = \frac{\hat{p}^2}{2} + K \cos(k\hat{x} - \alpha t) \sum_{n=1}^N \delta(t - nT), \quad (1)$$

where,  $\hat{p}$  and  $\hat{x}$  represent the momentum and position operators respectively. They obey canonical commutation relation  $[\hat{x}, \hat{p}] = i\hbar_{\text{eff}}$ , where the effective Planck constant  $\hbar_{\text{eff}}$  can be tuned in the experiment. Further,  $K$  is the stochastic parameter,  $T$  is the time period between consecutive kicks,  $k$  is the wave vector, and  $\alpha$  is the frequency difference between two lattice beams. The lattice velocity  $v$  arising from the frequency difference between the counter-propagating beams is  $v = \lambda\alpha$ , where  $\lambda$  is the wavelength of the optical lattice. Throughout this work, parameters will be chosen so that the classical analogue of QKR displays chaos, with  $K \geq 5$ . This parameter choice ensures that the localization effects we observe are of quantum origin.

As the quantum kicked rotor is time-periodic, the quantum dynamics can be conveniently analyzed through the period-1 Floquet operator

$$U = \exp\left(-i\frac{p^2 T}{2}\right) \exp(-iK \cos(kx - \alpha t)). \quad (2)$$

This evolves an initial state  $\psi(x, t = 0)$  over one kick period  $T$ , *i.e.*,  $\psi(x, T) = U\psi(x, 0)$  with the initial state chosen as a coherent state in position space given by

$$\psi(x, t = 0) = \frac{1}{\sqrt{2\pi}\sigma_w} \exp\left(-\frac{x^2}{2\sigma_w^2}\right) \exp(-ip_0 x), \quad (3)$$

and is consistent with the initial distribution of BEC. Here,  $\sigma_w$  characterizes the width of the wavefunction in position space, while  $p_0$  is the initial velocity, typically arising from launched velocity or micromotion. Generally, in our experiments, when BEC is launched with initial velocity  $p_0$ , the lattice velocity is stationary and vice

versa. In general, either moving the lattice appropriately or the atomic cloud imparted with initial velocity  $p_0$  in the lab frame are expected to induce similar effects [5, 39].

For numerical simulations, we use the standard split-operator method to evolve an initial state of the kicked rotor. This method consists of two primary components: the kick operator, which is diagonal in position space, and the free evolution operator, which is diagonal in momentum space. To simulate scenarios where the lattice is in motion in the lab frame, we imprint the phase just before each kick. Similarly, to model the situation in which BEC moves in the laboratory frame, we initialize the a wavefunction that incorporates the motion right from the outset.

### Asymmetric dynamical localization and micromotion

If the lattice is moved with constant velocity, then the kick potential (in the lab frame)  $V(x) = K \cos(kx - \alpha t)$  induces a path difference of  $\alpha T$  at each kick. Consequently, the corresponding phase difference between successive kicks is  $\phi = 2\pi\alpha T$  and this breaks the parity symmetry. The total phase difference accumulated after  $n$  kicks is  $\phi_n = 2\pi\alpha T \times (n - 1)$ , assuming that the phase is initialized to zero for the first kick. The accumulated phase difference  $\phi_n$  over short timescales induces an inhomogeneity in position space due to broken parity symmetry, leading to an asymmetric momentum distribution [5]. This asymmetry can be quantified through  $\langle p(t = 2T) \rangle$  immediately following  $n = 2$  kicks.

In the experiments, we control the lattice velocity by tuning  $\alpha$  and subsequently measure  $\langle p(t = 2T) \rangle$ . Based on physical consideration and since phases are unique only upto  $2\pi$ , we posit that the average momentum after two kicks to have a form

$$\langle p(t = 2T) \rangle = c \sin(2\pi\alpha T), \quad (4)$$

where  $c$  is a constant. This implies that if  $\alpha T = n/2$  (where  $n$  is an integer),  $\langle p \rangle = 0$  implying an absence of asymmetry for specific choice of initial velocity and kick period. In the long time limit of  $n \gg 1$ , the initial asymmetry accumulated in the short-time limit eventually freezes due to the emergence of dynamical localization. Hence, the early-time dynamics dictates the long-term behaviour and the onset of asymmetrical dynamical localization in the system.

For numerical simulations, we use the standard split-operator method to evolve an initial state of the kicked rotor. This method consists of two components: the kick operator (diagonal in position space), and the free evolution operator (diagonal in momentum space). To simulate scenarios where the lattice is in motion in the lab frame, the phase just before each kick is imprinted on the evolving wavefunction.

To gauge micromotion accurately, the optical lattice is

precisely moved with frequency difference of the order of 100Hz, aligning it with the scale of micromotion. Upon achieving a velocity for the lattice that corresponds precisely to the micromotion, we observe  $\langle p(t = 2T) \rangle$  equal to zero. This alignment establishes a direct correspondence between the velocity of the lattice and the velocity of micromotion.

### III. EXPERIMENTAL SETUP FOR QKR

The QKR setup we have used for this work is similar to the one described here [37]. However, instead of cold atoms, we utilize a BEC of  $^{87}\text{Rb}$  every 8 seconds, through forced evaporative cooling. The atoms are initially prepared in the  $|F = 1, m_F = -1\rangle$  state, with a BEC temperature of 80 nK and a population of approximately 40,000 atoms. This BEC serves as the initial wave function for our experimental investigations. The optical standing wave is produced using two independent laser beams, which are generated by a single laser passing through two separate acousto-optic modulators. We can control the frequency difference between lattice beams and their switching. Switching time and laser power provide us control over scaled Planck constant  $\hbar_{\text{eff}}$  and stochastic parameter  $K$ .

This work comprises two main components: probing asymmetric dynamical localization and measuring micromotion. To investigate localization phenomena, we implement the Bragg diffraction technique to launch the Bose-Einstein condensate (BEC) with varying recoil momentum, as outlined in [40]. By adjusting the frequency difference between the lattice beams and the on-time of the lattice beam, we achieve a good transfer of atoms to different momentum states. In our apparatus [41], a frequency difference of 15 kHz results in 2 recoil momenta, while a frequency difference of 30 kHz provides 4 recoil momenta, both have a fixed on-time of approximately  $\sim 66.6 \mu\text{s}$ . After the creation of the initial wave function of BEC with different velocities, we apply the usual kicked rotor pulse sequence to study the dynamical localization. In our QKR experiments, we maintain the stochastic parameter at  $K = 5$  and effective Planck constant at  $\hbar_{\text{eff}} = 4.6$  to ensure that the corresponding classical dynamics remains in the chaotic regime [3].

For the motion of the lattice, we generate a frequency difference ranging from 0 to 75 kHz between the lattice beams. This frequency range corresponds to a velocity range of 0 to 10 recoil momentum. We ensure that the kick strength remains constant across higher frequency regimes. The advantage of employing a moving lattice, rather than a moving BEC, lies in the flexibility to assign precise arbitrary velocities to the optical lattice from the laboratory frame. It also does not create any residual atoms in zeroth momentum state like in Bragg diffraction. Leveraging this control over micromotion, we scan the lattice velocity in a frequency range of  $-3$  to  $3$  kHz with increments of 100 Hz, enabling precise measurement

of micromotion BEC by balancing the relative motion.

## IV. ASYMMETRIC DYNAMICAL LOCALIZATION IN MOVING FRAME OF REFERENCE

In this section, we will consider two scenarios – (a) BEC launched with an initial momentum in a stationary lattice (called case-I), (b) BEC launched with zero initial momentum in a moving lattice (called case-II).

### 1. Case I: BEC moving in lab frame

In our experiment, BEC is launched with various recoil momenta,  $p_0 = n\hbar k$  ( $n \in \mathbb{Z}$ ), using Bragg diffraction. This is achieved by applying a pulse of length approximately  $66.6 \mu\text{s}$  to transfer all the population to the required momentum state, and appropriately adjusting the lattice power. Subsequently, free evolution period of approximately  $66.6 \mu\text{s}$  is allowed, corresponding to the Talbot time of the system. This ensures recreation of the initial wavefunction without any unintended phase accumulation [42]. Once the wavefunction with different velocities is created, it is subjected to periodic kicks to observe dynamical localization. The period of these kicks is set at  $T = 24.3 \mu\text{s}$ , corresponding to a scaled Planck constant of  $\hbar_{\text{eff}} = 4.6$ . The stochastic parameter is  $K = 5$  corresponding to a classical phase space that is almost fully chaotic [3, 37]. These parameters remain consistent throughout the paper unless stated otherwise.

Bose-Einstein Condensate is launched with initial momentum of  $p_0 = 0\hbar k, 2\hbar k$  and  $4\hbar k$  corresponding, respectively to, zero, two and four recoil photons. The momentum distributions observed after  $n = 30, 40,$  and  $50$  kicks are depicted in Fig. 1(a-c) respectively. In Fig. 1(a), standard symmetric dynamical localization pattern is observed for initial momentum  $p_0 = 0$ . Figure 1(b) illustrates an asymmetric dynamically localized momentum distribution peaked at  $2\hbar k$  when BEC is launched with  $p_0 = 2\hbar k$ . Similarly, in Fig. 1(c), dynamical localization is asymmetric with peak positioned at  $4\hbar k$ , corresponding to a launch momentum of  $p_0 = 4\hbar k$ . Asymptotically, as  $n \gg 1$ , the system remembers the initial momentum  $p_0$  since the maxima of the steady-state distribution occurs at  $p = |p_0|$ . As evident in Figs. 1(b,c), an asymmetry develops such that the localized momentum distribution in Fig. 1(b,c) has maxima at  $p = -p_0$ , when launched with initial momentum of  $p_0$ . In Fig. 1(b),  $\langle p \rangle$  with reference to initial given momentum  $p_0$ , is moving in the direction of the launched velocity, while in Fig. 1(c),  $\langle p \rangle$  is moving in the opposite direction of the launched velocity.

The bottom panel in Fig. 1 shows the corresponding results obtained from QKR simulations. The simulation results confirm the emergence of dynamical localization and evidently it is asymmetric for the case when BEC is launched with  $p_0 = 2\hbar k$  and  $p_0 = 4\hbar k$ . For  $p_0 = 2\hbar k$ ,

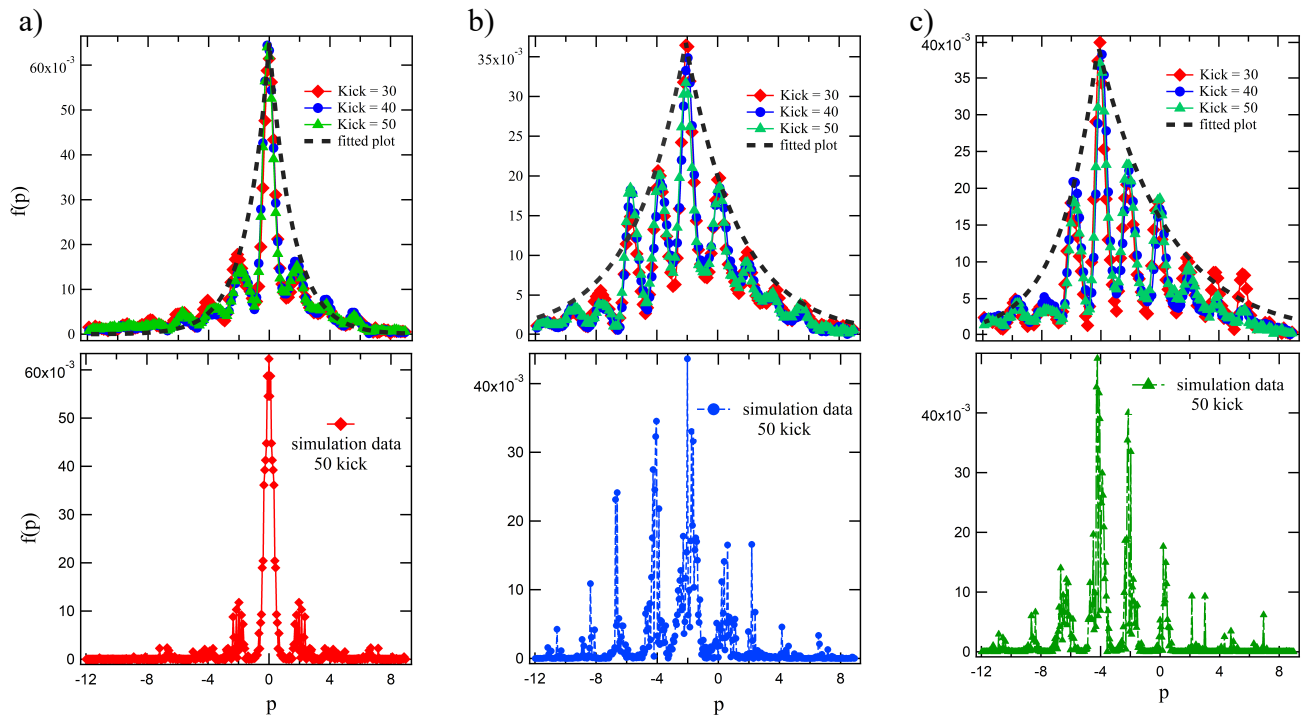


FIG. 1. Wavefunction profile for different launch velocity shown at 30, 40 and 50 kicks. In all the cases, dynamical localization has set in. Initial velocity corresponds to momenta (a)  $0\hbar k$ , (b)  $2\hbar k$ , and (c)  $4\hbar k$ . In all cases, in top panel, symbols are obtained experimental data. In bottom panel, symbols are obtained from kicked rotor simulations with 50 kicks.

the more population lies in the direction of the launched momentum and for  $p_0 = 4\hbar k$ , it lies in opposite direction, matching with the experimental result. The experimental profile in the vicinity of the peak value, in an average sense, is slightly elevated compared to simulation results (in both Figs. 1-2) in due to presence residual thermal atoms.

## 2. Case II: optical lattice moving in lab frame

In this section, we discuss moving the lattice in the lab frame by inducing a constant frequency difference  $\alpha$  in the range of 0 – 75 kHz, which spans almost 10 recoil momenta. After creating the BEC,  $100\mu s$  time-of-flight is allowed, and subsequently periodic kicks are applied. As seen in Figs. 2(a-b), dynamical localization is observed for various lattice velocities. For a direct comparison with case-I, optical lattice is moved with frequency difference 15 kHz and 30 kHz in the left direction, corresponding to  $2\hbar k$  and  $4\hbar k$  recoil momenta. The resulting steady-state momentum distribution after 50, 60 and 70 kicks is displayed in Figs. 2 (a-b). The asymmetry induced by the lattice motion is visible for 15 kHz and 30 kHz; for 15 kHz in Fig. 2(a) wave packet is moving in the same direction as a lattice (left direction), and for 30 kHz in Fig. 2(b), the wave packet is moving in the opposite direction of the lattice (left direction).

The bottom panel in Fig. 2 shows the correspond-

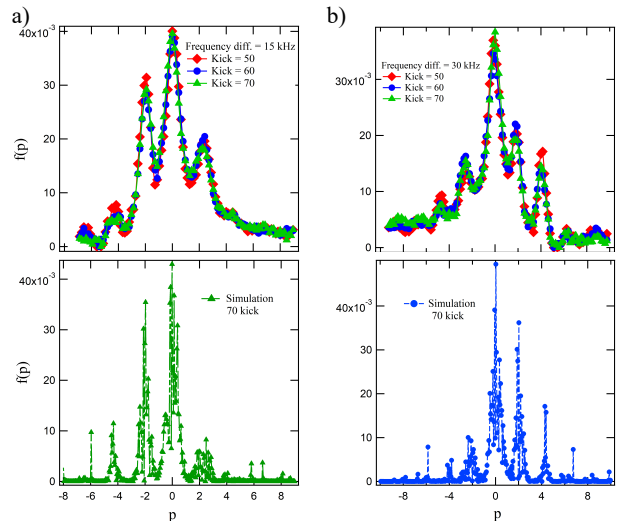


FIG. 2. Dynamically localization for two distinct frequency difference  $\alpha$ : (a) 15 kHz, (b) 30 kHz. (Top panel) experimental data shown as symbols for three different kick numbers, (bottom panel) simulation results shown as symbols at 70th kick.

ing localization pattern obtained from QKR simulations. The simulation results confirm the emergence of asymmetric dynamical localization when the optical lattice is moved by inducing a frequency difference of  $\alpha = 15$  kHz and  $\alpha = 30$  kHz.

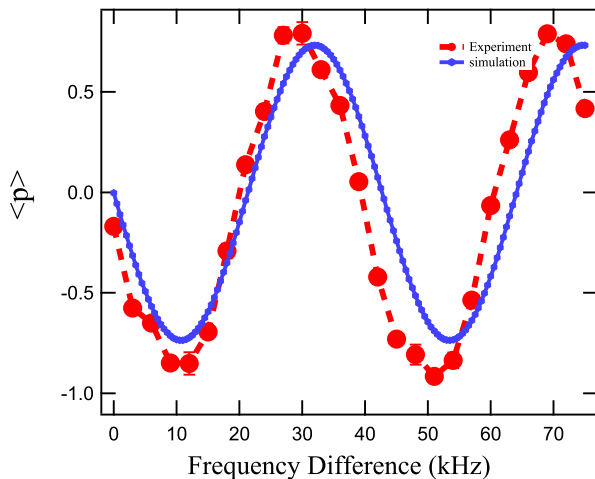


FIG. 3. Oscillatory behaviour of  $\langle p \rangle$  as a function of frequency difference (lattice velocity). In this experiment,  $\langle p \rangle$  is measured after two kicks.

### V. MEASUREMENT OF EARLY TIME DYNAMICS

To understand asymmetry induced by relative motion between the atomic cloud and the optical lattice, early-time dynamics after two kicks is analyzed. The optical lattice is moved by creating a frequency difference between two laser beams, ranging from 0 to 75 kHz. Subsequently, two kicks are applied separated by time interval  $T = 24.3 \mu\text{s}$  for different initial momenta  $p_0$  and  $\langle p \rangle$  is measured after a 10 ms time-of-flight. Remarkably, pronounced oscillations in  $\langle p \rangle$  are observed, consistent with Eq. 4. This is shown in Fig. 3, and suggests that  $\langle p \rangle$  exhibits a linear relationship in the limit of  $\alpha \rightarrow 0$ . This linearity provides a promising avenue to measure the micromotion discussed in Section VI. Figure 3 also shows simulation results (blue line), which agrees with the experimental results in the limit  $\alpha \rightarrow 0$ . For the large  $\alpha$ , where the lattice velocity is high, experiment deviates from the simulation due to finite pulse time.

Another intriguing feature observed in Fig. 3 is the difference in the sign of  $\langle p \rangle$  for 15 kHz (corresponding to two-recoil momentum) and 30 kHz (corresponding to four-recoil momentum). The opposite signs for  $\langle p \rangle$  in the early-time dynamics is a consequence of the asymmetric distribution observed after long-time evolution, as demonstrated in Section IV. In general, short time asymptotic carry the signature of the long-term behavior at other frequencies as well. In particular, for frequencies that are integer multiples of 21 kHz, asymmetry is absent in the distribution. This corresponds to the condition  $\alpha T = n/2$ . Irrespective of the speed of lattice, if the frequency difference is an integer multiple of 20.57 kHz, no asymmetry is expected to manifest in the distribution, as discussed in Eq. 4.

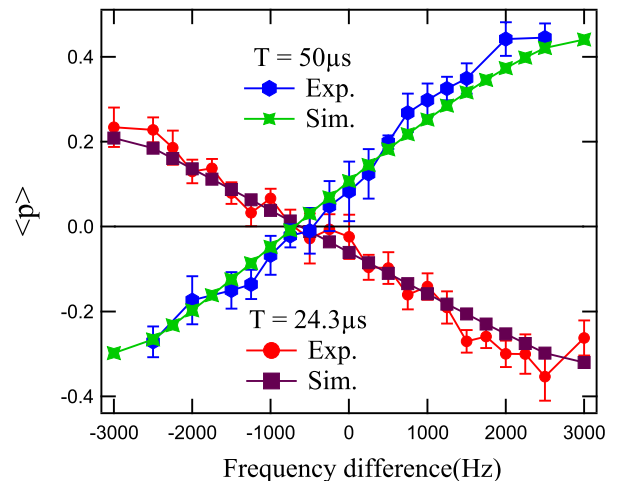


FIG. 4. Measured  $\langle p \rangle$  as a function of frequency difference  $\alpha$  for two different time delays. Micromotion of BEC is measured by scanning over a range of frequency differences. See text for details.

### VI. MEASUREMENT OF MICROMOTION OF BEC

Measuring the micromotion of the BEC poses a challenge due to its very small magnitude in the direction of the lattice [43]. This small magnitude of the velocity is difficult to measure accurately using conventional time-of-flight methods, which typically require long time-of-flight duration. One such measurement is performed in Ref. [21] through a 225 ms time-of-flight. To address this challenge and accurately measure micromotion, early-time measurements are conducted by systematically tuning  $\alpha$  of the lattice. A single-shot measurement can also measure micromotion if the lattice phase is stable. In these measurements, two different time delays,  $T = 24.3 \mu\text{s}$  and  $T = 50 \mu\text{s}$ , between two kicks, are employed.

The BEC micromotion is measured by tuning the lattice velocity in steps of frequency difference of 250 Hz, as illustrated in Fig. 4. The phase evolution induced by micromotion is effectively balanced by the lattice motion. When the net average momentum  $\langle p \rangle = 0$ , the BEC micromotion velocity can be deduced from the corresponding frequency difference. The calculated frequency difference at points of  $\langle p \rangle = 0$  are  $(590 \pm 45) \text{ Hz}$ , corresponding to a velocity of  $(460 \pm 35) \mu\text{m/s}$  for  $T = 24.3 \mu\text{s}$ , and  $(649 \pm 24) \text{ Hz}$ , corresponding to a velocity of  $(506 \pm 19) \mu\text{m/s}$  for  $T = 50 \mu\text{s}$ . The micromotion can also be obtained by measuring asymmetry, keeping the frequency difference at  $\alpha = 0$ , if the proportionality constant  $c$  of Eq. 4 is known. However, former method is highlighted as it offers a direct and precise measurement of the micromotion.

## VII. CONCLUSION

This work gives insights about the nature of dynamical localization when a wavefunction is launched with initial momenta  $p_0 \neq 0$  in the lab frame as well as when the optical lattice is moved in lab frame. In both scenarios, after a short diffusive timescale, the wavefunction is localized with an asymmetric distribution profile. This asymmetry emerges during the early time dynamics – driven by the breaking of parity symmetry due to the motion of the wavefunction or lattice. This feature is employed for precisely measuring the micromotion of the BEC. For the parameters of the experimental system we employed, velocity measurement yielded  $(460 \pm 35) \mu\text{m/s}$  in our system. This micromotion measurement is crucial for precision instruments such as atom interferometers and atomic gyroscopes, as micromotion can introduce systematic shifts and uncertainties in their mea-

surements. The micromotion velocity is an order of magnitude smaller than the one recoil photon momentum, as well as mean velocity associated with BEC temperature. By utilizing the broken parity symmetry due to micromotion, measurement of such a small velocity is possible. Further, it might not be significantly affected by velocity distribution of the BEC, a common challenge in spectroscopy technique. This work contributes to our understanding of the precision measurement based on broken parity symmetry.

## VIII. ACKNOWLEDGMENTS

S.S.M. acknowledge a research fellowship from Council of Scientific and Industrial Research (CSIR), Government of India. All the authors thank the National Mission on Interdisciplinary Cyber Physical Systems for funding from the DST, Government of India through the I-HUB Quantum Technology Foundation, IISER-Pune.

- 
- [1] B. Gadway, J. Reeves, L. Krinner, and D. Schneble, Evidence for a quantum-to-classical transition in a pair of coupled quantum rotors, *Phys. Rev. Lett.* **110**, 190401 (2013).
- [2] J. H. S. Toh, M. Du, X. Tang, Y. Su, T. Rojo, C. O. Patterson, N. R. Williams, C. Zhang, and S. Gupta, Evidence for a many-body anderson metal-insulator transition using kicked quantum gases, arXiv preprint arXiv:2305.14817 <https://doi.org/10.48550/arXiv.2305.14817> (2023).
- [3] J. H. See Toh, K. C. McCormick, X. Tang, Y. Su, X.-W. Luo, C. Zhang, and S. Gupta, Many-body dynamical delocalization in a kicked one-dimensional ultracold gas, *Nature Physics* **18**, 1297 (2022).
- [4] A. Cao, R. Sajjad, H. Mas, E. Q. Simmons, J. L. Tanlimco, E. Nolasco-Martinez, T. Shimasaki, H. E. Kondakci, V. Galitski, and D. M. Weld, Interaction-driven breakdown of dynamical localization in a kicked quantum gas, *Nature Physics* **18**, 1302 (2022).
- [5] I. Dana, V. Ramareddy, I. Talukdar, and G. S. Summy, Experimental realization of quantum-resonance ratchets at arbitrary quasimomenta, *Phys. Rev. Lett.* **100**, 024103 (2008).
- [6] M. Sadgrove, M. Horikoshi, T. Sekimura, and K. Nakagawa, Rectified momentum transport for a kicked bose-einstein condensate, *Phys. Rev. Lett.* **99**, 043002 (2007).
- [7] R. Sajjad, J. L. Tanlimco, H. Mas, A. Cao, E. Nolasco-Martinez, E. Q. Simmons, F. L. N. Santos, P. Vignolo, T. Macrì, and D. M. Weld, Observation of the quantum boomerang effect, *Phys. Rev. X* **12**, 011035 (2022).
- [8] L. Tessieri, Z. Akdeniz, N. Cherroret, D. Delande, and P. Vignolo, Quantum boomerang effect: Beyond the standard anderson model, *Phys. Rev. A* **103**, 063316 (2021).
- [9] J. Janarek, B. Grémaud, J. Zakrzewski, and D. Delande, Quantum boomerang effect in systems without time-reversal symmetry, *Phys. Rev. B* **105**, L180202 (2022).
- [10] S. Dadras, A. Gresch, C. Groiseau, S. Wimberger, and G. S. Summy, Quantum walk in momentum space with a bose-einstein condensate, *Phys. Rev. Lett.* **121**, 070402 (2018).
- [11] K. Bongs, M. Holynski, J. Vovrosh, P. Bouyer, G. Condon, E. Rasel, C. Schubert, W. P. Schleich, and A. Roura, Taking atom interferometric quantum sensors from the laboratory to real-world applications, *Nature Reviews Physics* **1**, 731 (2019).
- [12] C. F. Ockeloen, R. Schmied, M. F. Riedel, and P. Treutlein, Quantum metrology with a scanning probe atom interferometer, *Phys. Rev. Lett.* **111**, 143001 (2013).
- [13] K. S. Hardman, P. J. Everitt, G. D. McDonald, P. Manju, P. B. Wigley, M. A. Sooriyabandara, C. C. N. Kuhn, J. E. Debs, J. D. Close, and N. P. Robins, Simultaneous precision gravimetry and magnetic gradiometry with a bose-einstein condensate: A high precision, quantum sensor, *Phys. Rev. Lett.* **117**, 138501 (2016).
- [14] A. Peters, K. Y. Chung, and S. Chu, High-precision gravity measurements using atom interferometry, *Metrologia* **38**, 25 (2001).
- [15] Z.-K. Hu, B.-L. Sun, X.-C. Duan, M.-K. Zhou, L.-L. Chen, S. Zhan, Q.-Z. Zhang, and J. Luo, Demonstration of an ultrahigh-sensitivity atom-interferometry absolute gravimeter, *Phys. Rev. A* **88**, 043610 (2013).
- [16] P. Berg, S. Abend, G. Tackmann, C. Schubert, E. Giese, W. P. Schleich, F. A. Narducci, W. Ertmer, and E. M. Rasel, Composite-light-pulse technique for high-precision atom interferometry, *Phys. Rev. Lett.* **114**, 063002 (2015).
- [17] I. Dutta, D. Savoie, B. Fang, B. Venon, C. L. Garrido Alzar, R. Geiger, and A. Landragin, Continuous cold-atom inertial sensor with 1 nrad/sec rotation stability, *Phys. Rev. Lett.* **116**, 183003 (2016).
- [18] M.-K. Zhou, Z.-K. Hu, X.-C. Duan, B.-L. Sun, J.-B. Zhao, and J. Luo, Precisely mapping the magnetic field gradient in vacuum with an atom interferometer, *Phys.*

- Rev. A* **82**, 061602 (2010).
- [19] R. Bouchendira, P. Cladé, S. Guellati-Khélifa, F. m. c. Nez, and F. m. c. Biraben, New determination of the fine structure constant and test of the quantum electrodynamics, *Phys. Rev. Lett.* **106**, 080801 (2011).
- [20] S.-Y. Lan, P.-C. Kuan, B. Estey, P. Haslinger, and H. Müller, Influence of the coriolis force in atom interferometry, *Phys. Rev. Lett.* **108**, 090402 (2012).
- [21] K. S. Hardman, A bec based precision gravimeter and magnetic gradiometer: design and implementation [10.25911/5d723b873573a](https://arxiv.org/abs/10.25911/5d723b873573a) (2016).
- [22] J. Stenger, S. Inouye, A. P. Chikkatur, D. M. Stamper-Kurn, D. E. Pritchard, and W. Ketterle, Bragg spectroscopy of a bose-einstein condensate, *Phys. Rev. Lett.* **82**, 4569 (1999).
- [23] J. Ringot, P. Szriftgiser, and J. C. Garreau, Subrecoil raman spectroscopy of cold cesium atoms, *Phys. Rev. A* **65**, 013403 (2001).
- [24] P. H. Jones, M. Goonasekera, H. E. Saunders-Singer, and D. R. Meacher, Shifting the boundaries: Pulse-shape effects in the atom-optics kicked rotor, *Europhysics Letters* **67**, 928 (2004).
- [25] M. Arnal, G. Chatelain, C. Cabrera-Gutiérrez, A. Fortun, E. Michon, J. Billy, P. Schlagheck, and D. Guéry-Odelin, Beyond effective hamiltonians: Micromotion of bose-einstein condensates in periodically driven optical lattices, *Phys. Rev. A* **101**, 013619 (2020).
- [26] J. Sun, R. Liao, P. Zhao, Z. Hu, Z. Wang, X.-J. Liu, X. Zhou, and X. Chen, A quantitative study of the micromotion of a p-band superfluid in a shaking lattice, *Journal of Physics B: Atomic, Molecular and Optical Physics* **56**, 095302 (2023).
- [27] J. Mangaonkar, C. Vishwakarma, S. S. Maurya, S. Sarkar, J. L. MacLennan, P. Dutta, and U. D. Rapol, Effects of finite momentum width on the reversal dynamics in a bec based atom optics  $\delta$ -kicked rotor, *Journal of Physics B: Atomic, Molecular and Optical Physics* **53**, 235502 (2020).
- [28] S. Chai, J. Fekete, and M. F. Andersen, Measuring the local gravitational field using survival resonances in a dissipatively driven atom-optics system, *Phys. Rev. A* **98**, 063614 (2018).
- [29] R. Dubertrand, I. Guarneri, and S. Wimberger, Fidelity for kicked atoms with gravity near a quantum resonance, *Phys. Rev. E* **85**, 036205 (2012).
- [30] F. M. Izrailev, Simple models of quantum chaos: Spectrum and eigenfunctions, *Physics Reports* **196**, 299 (1990).
- [31] M. Santhanam, S. Paul, and J. B. Kannan, Quantum kicked rotor and its variants: Chaos, localization and beyond, *Physics Reports* **956**, 1 (2022).
- [32] F. L. Moore, J. C. Robinson, C. Bharucha, P. E. Williams, and M. G. Raizen, Observation of dynamical localization in atomic momentum transfer: A new testing ground for quantum chaos, *Phys. Rev. Lett.* **73**, 2974 (1994).
- [33] S. Fishman, D. R. Grempel, and R. E. Prange, Chaos, quantum recurrences, and anderson localization, *Phys. Rev. Lett.* **49**, 509 (1982).
- [34] F. L. Moore, J. C. Robinson, C. F. Bharucha, B. Sundaram, and M. G. Raizen, Atom optics realization of the quantum  $\delta$ -kicked rotor, *Phys. Rev. Lett.* **75**, 4598 (1995).
- [35] P. H. Jones, M. Goonasekera, D. R. Meacher, T. Jonckheere, and T. S. Monteiro, Directed motion for delta-kicked atoms with broken symmetries: Comparison between theory and experiment, *Phys. Rev. Lett.* **98**, 073002 (2007).
- [36] A. Kenfack, J. Gong, and A. K. Pattanayak, Controlling the ratchet effect for cold atoms, *Phys. Rev. Lett.* **100**, 044104 (2008).
- [37] S. S. Maurya, J. B. Kannan, K. Patel, P. Dutta, K. Biswas, J. Mangaonkar, M. S. Santhanam, and U. D. Rapol, Interplay between quantum diffusion and localization in the atom-optics kicked rotor, *Phys. Rev. E* **106**, 034207 (2022).
- [38] C. Hainaut, A. Rançon, J.-F. m. c. Clément, J. C. Garreau, P. Szriftgiser, R. Chicireanu, and D. Delande, Ratchet effect in the quantum kicked rotor and its destruction by dynamical localization, *Phys. Rev. A* **97**, 061601 (2018).
- [39] M. Lepers, V. Zehnlé, and J. C. Garreau, Kicked-rotor quantum resonances in position space: application to situations of experimental interest, *The European Physical Journal D* **63**, 449 (2011).
- [40] S.-w. Chiow, T. Kovachy, H.-C. Chien, and M. A. Kasevich,  $102\hbar k$  large area atom interferometers, *Phys. Rev. Lett.* **107**, 130403 (2011).
- [41] P. Dutta, S. S. Maurya, K. Patel, K. Biswas, J. Mangaonkar, S. Sarkar, and U. D. Rapol, A decade of advancement of quantum sensing and metrology in india using cold atoms and ions, *Journal of the Indian Institute of Science* **103**, 609 (2023).
- [42] J. Ni, W. K. Lam, S. Dadras, M. F. Borunda, S. Wimberger, and G. S. Summy, Initial-state dependence of a quantum resonance ratchet, *Phys. Rev. A* **94**, 043620 (2016).
- [43] Y. Ben-Aïcha, Z. Mehdi, C. Freier, S. S. Szigeti, P. B. Wigley, L. O. Conlon, R. Husband, S. Legge, R. H. Eagle, J. J. Hope, N. P. Robins, J. D. Close, K. S. Hardman, S. A. Haine, and R. J. Thomas, A dual open atom interferometer for compact, mobile quantum sensing (2024), [arXiv:2405.00400](https://arxiv.org/abs/2405.00400) [quant-ph].